MSc in Photonics

PHOTONICS**BCN**

Universitat Politècnica de Catalunya (UPC)
Universitat Autònoma de Barcelona (UAB)
Universitat de Barcelona (UB)
Institut de Ciències Fotòniques (ICFO)

http://www.photonicsbcn.eu

Master in Photonics

MASTER THESIS WORK

DEVELOPMENT OF A NEW MULTISPECTRAL IMAGING SYSTEM CONSISTING OF A LIQUID CRYSTAL TUNABLE FILTER

Raquel García Rodríguez

Supervised by Dr. Jaume Pujol and Meritxell Vilaseca, (CD6)

Presented on date 5th September 2013

Registered at

Escola Tècnica Superior d'Enginyeria de Telecomunicació de Barcelona

Development of a New Multispectral Imaging System consisting of a Liquid Crystal Tunable Filter

Raquel García Rodríguez
Centre de Desenvolupament de Sensors, Instrumentació i Sistemes (CD6),
Universitat Politècnica de Catalunya (Terrassa - Barcelona, Spain).

E-mail: rgr.valtuille@gmail.com

Abstract. The aim of this study was to develop a new portable multispectral system basically composed of a monochrome digital camera, a liquid crystal tunable filter (LCTF) and a laptop. The system had a high spatial resolution (pixels of the camera) as well as a high spectral resolution, which was determined by the number of available spectral bands (from 400 to 720 nm with a 10-nm step). The software to control the system was developed, and its physical properties, especially the transmission of the spectral bands and the spatial uniformity, were characterized. Furthermore, the optimal objective lens was selected according to the desired requirements (field of view, angle-of-acceptance etc.). Using the developed setup, multispectral images of several scenes were captured and the spectral radiance and reflectance on any pixel were computed. This novel system is a good alternative to conventional spectrophotometers when high spatial resolution is required, nevertheless some arrangements are still needed to improve its performance.

Keywords: multispectral systems, liquid crystal device, tunable filter.

1. Introduction

Multispectral imaging systems are becoming an essential tool due to the large amount of information that they provide from the scene under study. They have a great variety of utilities and there are many fields in which they can be employed: color reproduction, painting conservation, medicine, chemical and pharmaceutical industries, analysis of food, agriculture, etc. Multispectral systems collect the reflected light of the imaged object at different wavelengths, which is the result of the interaction of the incident photons of the light source with the surface atoms, and thus relevant information about its surface properties is obtained [1]. Multispectral systems generate a set of images, where each one represents a spectral band of the electromagnetic spectrum. These images are then combined and form a three-dimensional spectral data cube, with spatial (X, Y) but also spectral information (λ) (Figure 1).

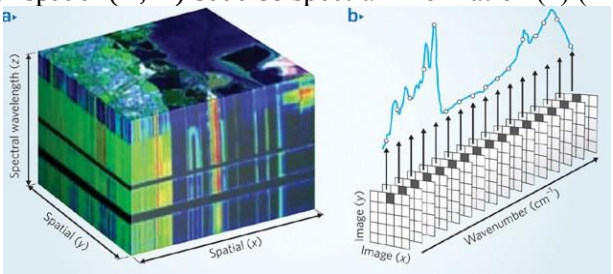

Figure 1. a) Spectral data cube and b) spectral data provided for one pixel (Source: Bannon, 2009 [2]).

Until few years ago, spectral analysis was conventionally carried out by using spectrophotometers, which are able of analyzing only small areas due to the fact that they use a

photodiode as a sensor. Furthermore, these areas are supposed to be uniform in terms of photometric and colorimetric properties since the light coming from them is integrated at the sensor. In contrast, multispectral systems provide spectral information for each pixel of an image since they include a digital camera.
One significant key in the designing process of these systems is how to implement the capture of the third dimension which should be synthesized over time, since the cameras are able of capturing just two dimensions simultaneously [1]. The first approach is to implement a system based on a scanning line, i. e. the pushbroom configuration, which includes a spectrograph in front of a digital camera and takes the spectral information line by line being necessary to linearly move the object to complete the sequence. The second approach is the whiskbroom configuration, with only one detector which accumulates the spectral data of each pixel doing a bidimensional (X, Y) spatial scanning [3]. The third approach involves the use of narrowband filters which are capable of transmitting light only for specific wavelengths. In this case, a spectral image with the whole spatial information (X, Y) is captured for each channel of the system. By stacking together these images from the same area, the spectral cube is built. The filters often used are interference filters placed in a filter wheel or tunable acousto-optic (AOTF) or liquid crystal filters (LCTF).
A LCTF is basically a device whose spectral transmission can be controlled by varying the voltage [4]. The structure relies on constructive and destructive interference effects in a multi-layer stack of quarter-wave reflective layers and half-wave spacer layers. As shown schematically in Figure 2, each cell consists of an initial linear polarizer followed by a birrefringent quartz element of fixed retardance; then a liquid-crystal waveplate permits to obtain a variable retardance thanks to two transparent electrodes placed at each side of the plate, which create a variable electrical field depending on the wavelength chosen; finally there is an analyzer oriented with its axis parallel to the initial polarizer [5]. The superposition of several of these layers allows the filter to obtain monochromatic light.

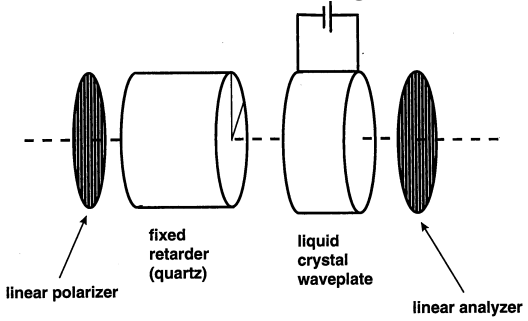

Figure 2. Schematic representation of a LCTF cell (Source: Araujo P 2007 [5]).

The aim of this study is to develop a new multispectral imaging system mainly composed of a monochrome digital camera and a visible LCTF, all connected to a laptop. The multispectral imaging system must be robust and portable and it should be as fast as possible in collecting the spectral cube of the scene. The system must provide the spectral radiance and reflectance of the captured scene pixel by pixel.
The paper is structured as follows: in the following section the setup used is detailed as well as its advantages and limitations. Afterwards some experiments that have been carried out in order to characterize the multispectral system are shown. Next, the methods used for the image acquisition as well as subsequent processing and analysis to compute radiance and reflectance values are described. Finally, the results achieved in terms of radiance and reflectance are presented together with the main conclusions.

2. Experimental setup

2.1. Components and complexity of the multispectral system design

The multispectral imaging system consisted of a cooled 12-bit depth CCD monochrome digital camera (QImaging QICAM Fast 1394) with 1392 x 1040 pixels (pixel size: 4.65µm x 4.65µm)

assembled to an objective achromatic lens (FA 2/3" F1.6/25 mm), an LCTF (Varispec filter model #VIS-07-HC-20-1012) and an infrared (IR) cutoff filter (Edmund Optics #55-234). The system was controlled by a laptop (Figure 3):

Figure 3. Multispectral system.

The LCTF employed in this study had a fixed spectral bandwidth of 10 nm, with a central wavelength electronically tunable to any wavelength between 400 and 720 nm. The working aperture diameter was of 22 mm and the angle-of-acceptance of light specified by the manufacturer was of 7.5 degrees (half-angle).

One of the most relevant aspects in the system design is where to place the tunable filter: between the lens and the camera (BLC) or in front of the lens (FOL). The benefit to the BLC method is that the filter is protected by lenses on both sides. The drawback is that it requires a very specific optical design since the lens is located very far from the sensor (the thickness of the filter is about 50 mm), and thus conventional manufactured focal distances are not appropriate. In contrast, the FOL method requires less optical integration and conventional lenses can be used instead. The drawback to the FOL method is that the position of the filter may interfere with easy operation of the lens. In this work, we chose the FOL configuration since it was the most practical and inexpensive method. Although it provided an easy implementation, it also presented some limitations: since a large field of view was required, a very short focal length was attempted to be used. But then image vignetting was observed because of the small aperture diameter of the filter (22 mm) as well as its thickness (50 mm).

This, together with the fact that the maximum allowed angle-of-acceptance of the LCTF was of 7.5º and considering the sensor size and other optical factors such as the depth of focus, the shortest focal length that could finally be used was of 25 mm.

Another factor to be considered was the chromatic aberration caused by being working with light coming from different spectral bands, which were focused at different distances depending on their wavelength.

To minimize this effect as much as possible and to avoid blurred images at the extreme bands, the objective lens chosen was achromatic and the central channel (550 nm) was firstly focused, keeping this configuration for all subsequent measures. Moreover the F-number (F#) was kept as high as possible to ensure the largest possible depth of focus. However this was a compromise between the diaphragm aperture and the amount of light reaching the sensor, which was very low at short wavelengths due to the low transmission of the LCTF (see next section).

Finally, another key aspect was the use of an IR cutoff filter. As it will be seen later, when bluish channels of the LCTF were selected (400-450 nm), second order peaks of transmittance appeared in the red and near IR region. This effect was eliminated by placing an IR cutoff filter (750-1000 nm) in front of the LCTF (Figure 4).

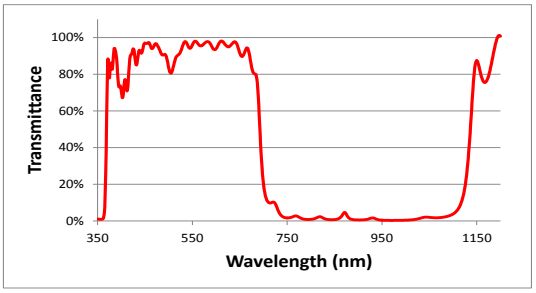

Figure 4. Spectral transmittance of the IR cutoff filter (Edmund Optics #55-234).

2.2. LCTF transmittance characterization

A setup including a conventional spectrophotometer (Instrument Systems Spectro 320 R5) and a halogen lamp with a power supply was used to characterize the transmittance of each channel of the LCTF from 400 to 720 nm with a 10-nm step (Figure 5). There were noticeable discrepancies between the transmittances

measured and those given by the manufacturer, which were much higher. The maximum peaks (around 30% of transmittance) were measured at 700-720 nm, while for wavelengths below 450 nm the maximum transmittances were lower than 5%. All this together with the fact that CCD cameras had a non-constant sensitivity means that a suitable exposure time for each spectral band was used to guarantee as much as possible an acceptable signal-to-noise ratio. However noise problems still arose at short wavelengths due to the low sensitivity of the system in this region.

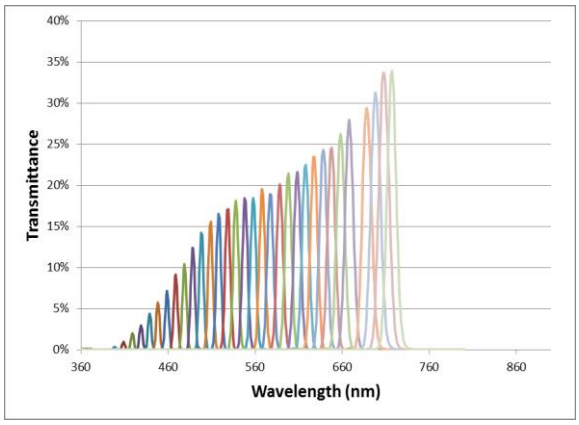

Figure 5. LCTF spectral transmittances.

On the other hand Figure 6 (a) shows the second order undesirable red and near IR peaks that appeared when blue wavelengths were selected (400-450 nm). As already mentioned an IR filter was used to remove them (750-1000 nm). The red peaks below 750 nm could not be avoided since they overlapped with other LCTF visible channels and were assumed as an error of the system. Moreover, despite there were more peaks beyond 1000 nm, the CCD camera was not capable of capturing them due to its low sensitivity in that region.

The last issue considered was the influence on the transmittance of the angle-of-incidence of light. This angular dependence implies a non-homogeneous light transmission, being maximum at the center of the image and decreasing towards the periphery. Figure 6 (b) shows the transmittance decrease for three angles of incidence of light: 0, 5 and 10 degrees. This effect was partially corrected in the setup by applying an algorithm for the correction of the spatial non-uniformity (see section 3.2).

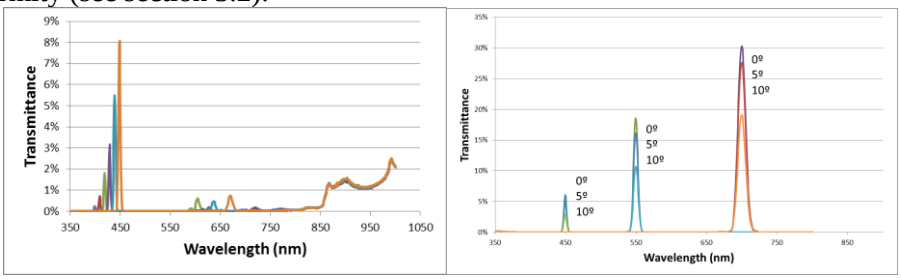

(a) (b)

Figure 6. (a) Red and near IR peaks of transmittance when the LCTF is working in the blue region. (b) Influence of the angle-of-incidence in the transmittance. Profiles for angles of 0º, 5º and 10º are plotted, showing a transmittance decrease with the angle.

2.3. Linearity of the system response

The fundamental function of a CCD camera is to convert the incident photons arriving at the sensor into pairs of electrons [5]. A good camera performance implies the linearity of its response. This means that the outreaded pixel intensity in terms of digital levels must be proportional to the number of incident photons. In this study this was checked for several representative channels located along the system: 450, 550, and 650 nm.

The exposure time was changed while all the other parameters were kept constant and the linear range of the system response was experimentally determined.

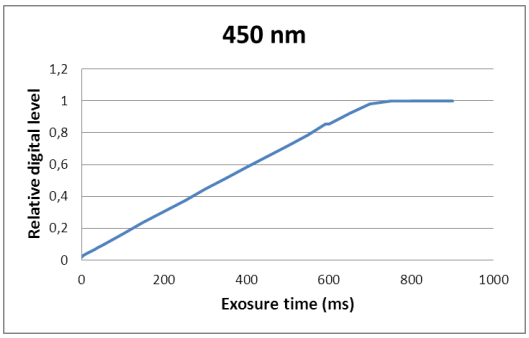

Figure 8. Study of the linearity of the system for the 450-nm spectral band.

The setup used for this purpose involved measurements of a calibrated standard white plate (Gigahertz-Optik GmbH BN-R98-SQ12) in a cabin booth (Verivide CAC 120) illuminated with a uniform light source emulating D65. Then the average of the digital levels of all pixels as a function of the exposure time was plotted. Figure 8 shows the results of linearity obtained for the 450 nm spectral band.

2.4. Temporal and spatial noise correction

There are many inherent noise sources in the developed multispectral system caused by b3oth the CCD camera and the LCTF. Noise sources can be classified in two main groups: temporal and spatial. The first group can be easily corrected by averaging several images taken under the same conditions. In this study temporal noise correction was carried out by averaging 10 images [6]. On the other hand, the spatial noise mainly refers to the non-homogeneity in the response of the pixels of the camera as well as the heterogeneous transmittance of the LCTF.

Figure 9 shows an image corresponding to the calibrated standard white plate uniformly illuminated. As it can be seen, there is an important lack of spatial uniformity in the response of the system, which can be fundamentally attributed to the LCTF transmittance, although some vignetting and the camera also play a role.

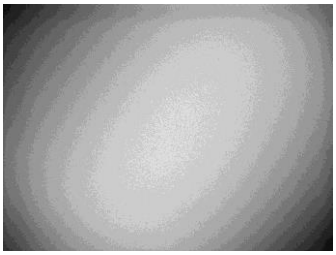

Figure 9. Image corresponding to a calibrated standard white plate showing the lack of uniformity in the response of the system.

In this study a spatial non-uniformity correction or flat-field correction was applied to correct this effect [6].

Basically two variants of the correction were applied, both requiring two images: a dark image captured with the same exposure time that the image to be corrected and with the objective lens covered, and a uniform flat-field image. In the first variant, the dark image and the flat-field image are combined with the image to be corrected according to the following equation:

$$DL_c(i,j) = k\,\frac{DL(i,j) - DL_0(i,j)}{DL_B(i,j) - DL_0(i,j)} \tag{1}$$

where $DL_c(i,j)$, $DL(i,j)$, $DL_0(i,j)$ y $DL_B(i,j)$ are the digital levels at the (i,j) pixel of the corrected image, the original or raw non-corrected image, the dark image, and the flat-field correction image, respectively, and k is a calibration constant.

The second variant is based on the calculation of gain and offset matrixes given by:

$$\begin{aligned} DL_c(i,j) &= O(i,j) + G(i,j)DL(i,j) \\ G(i,j) &= \frac{DL_B - DL_0}{DL_B(i,j) - DL_0(i,j)} \\ O(i,j) &= DL_0 - G(i,j)DL_0(i,j) \end{aligned} \tag{2}$$

where $O(i,j)$ (i = 1,…, m and j = 1,…, n) represents the (i,j) element of the correction offset matrix O, $G(i,j)$ represents the (i,j) element of the correction gain matrix G, and DL_0 and DL_B are the called reference digital levels of the dark image and the flat-field correction image, respectively. The mean digital level for all of the image's pixels is used as the reference digital level.

3. Method

3.1. Image acquisition

In this study, all the images acquired with the multispectral system were taken under the same conditions. The samples to be analysed were placed inside a specially designed cabin booth which provided a homogeneous illumination over the samples. The distance between them and the imaging system was of 58 cm approximately (Figure 10) achieving a field of view of 13 × 17 cm. Regarding the objective lens, a F# of 2 and a focus distance of approximately 0.7 m were used, and the central channel of the system (550 nm) was always focused at the beginning of the acquisition process. The focus distance and working distance are not exactly the same due to the

depth of focus present in the system caused by the pixel size and the optical properties of the objective lens such as the diaphragm aperture. The customizable parameters of the camera were set to the following values: a gain value of 10 and an offset value of 2200.

Figure 10. Image acquisition setup.

The exposure time of each spectral band was selected in order to obtain the maximum mean DL with non-saturated pixels when imaging the standard calibrated white plate (See Table 1). This allowed adjusting the dynamic range of the system regarding the amount of light. Once the configuration of the setup was defined, an acquisition process scanning from 400 to 720 nm with a 10-nm step was carried out for the samples analysed, thus obtaining the corresponding spectral cube.

Table 1. Exposure time (T) used for each spectral band (λ) and the mean digital levels (mDL) obtained for the calibrated standard white plate without any pixel saturated.

λ(nm)	**400**	**410**	**420**	**430**	**440**	**450**	**460**	**470**
T(ms)	30000	8000	2700	1250	510	355	213	158
mDL	2528	2497	2629	2512	2509	2506	2589	2603
λ(nm)	**480**	**490**	**500**	**510**	**520**	**530**	**540**	**550**
T(ms)	116	104	94	94	84.8	77	70	50
mDL	2554	2598	2541	2548	2502	2533	2499	2497
λ(nm)	**560**	**570**	**580**	**590**	**600**	**610**	**620**	**630**
T(ms)	79	78	64	72	75	72	68	60
mDL	2508	2519	2455	2500	2602	2609	2601	2598
λ(nm)	**640**	**650**	**660**	**670**	**680**	**690**	**700**	**710**	**720**
T(ms)	60	54	47	69	104	135	244	700	1408
mDL	2599	2602	2601	2596	2591	2467	2368	2404	2549

The samples captured in this study were five standardized colour patches belonging to the X-Rite Munsell CCCR ColorChecker® Classic chart (Figure 11). Images of the calibrated standard white plate as well as dark images were also captured with the same conditions at the end of the process, since they were later used in the non-uniform spatial correction of the system. Finally, the true radiance ($W/m^2 \cdot sr$) corresponding to each of the analysed samples was also measured using a standard spectroradiometer (PhotoResearch PR655). The true reflectance of the samples was calculated by computing the ratio between the radiance of the sample and that of the calibrated white plate.

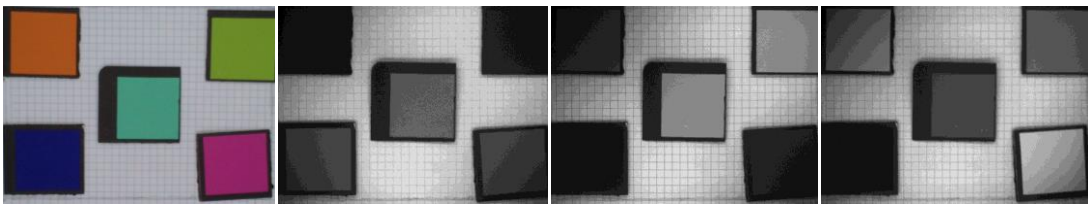

Figure 11. From left to right: RGB image of the scene and spectral images captured with the multispectral system corresponding to 450 nm, 550 nm and 690 nm. The samples can be seen in each image: Orange (top-left), yellow green (top-right), bluish green (centre), blue (bottom-left) and magenta (bottom-right).

3.2. Image processing

As already mentioned, the aim of this study was to reconstruct the spectral radiance and reflectance of the analysed samples pixel by pixel. Both quantities were computed by using the two variants of the non-uniform correction algorithm as established in section 2.4.

In the case of calculating the radiance by means of variant I, the constant *k* of Eq. (1) was established as the spectral radiance ($W/m^2 \cdot sr \cdot nm$) of the calibrated standard white plate measured with the spectroradiometer PR655 for each evaluated wavelength. This measurement was taken at the centre of the image but as already described, the radiance over the whole field of view was rather uniform. The image corresponding to the calibrated white plate was used as base or flat-field correction image. For reflectance calculations, *k* was set to the spectral reflectance value provided by the manufacturer of the calibrated standard white plate.

$$Rad(i,j) = S_{PR655} \frac{DL(i,j) - DL_0(i,j)}{DL_B(i,j) - DL_0(i,j)} \quad (3)$$

$$Refl(i,j) = R_{Gi} \frac{DL(i,j) - DL_0(i,j)}{DL_B(i,j) - DL_0(i,j)} \quad (4)$$

Where *Rad(i,j)* is the spectral radiance ($W/m^2 \cdot sr \cdot nm$) estimated by means of the multispectral system for each wavelength, S_{PR655} is the spectral radiance of the calibrated standard white plate measured with the spectroradiometer PR655 for each wavelength, *Refl(i,j)*is the spectral reflectance estimated by means of the multispectral system for each wavelength, and R_{Gi} is the spectral reflectance of the calibrated standard white plate provided by the manufacturer.
In the case of using variant II, the spectral radiances were calculated with the following equation:

$$Rad(i,j) = \frac{S_{PR655}}{DL_{BC}} DL_c(i,j) \quad (5)$$

Where $DL_C(i,j)$ is the corrected image by means of the method described in Eq. (2) and DL_{BC} is the digital level corresponding to the calibrated standard white plate once corrected, which is equal to the mean digital level of the uncorrected image.
In the case of the reflectance, the same equation was used but using R_{Gi} instead of S_{PR655}.

3.3. Evaluation of the estimated radiances and reflectances

In order to evaluate the differences between the true radiance (reflectance) and the estimated one by means of the multispectral system, different metrics were used.
First of all, the CIELAB colour difference formula proposed by the CIE (International Commission on Illumination) in 1976 was used. This formula computes the difference between two colours, specified by [L^*_1, a^*_1, b^*_1] and [L^*_2, a^*_2, b^*_2], as the Euclidean distance between them in the CIELAB space [7]:

$$\Delta E = \sqrt{\Delta L^2 + \Delta a^2 + \Delta b^2} \quad (6)$$

Where L* is the lightness of a colour and its scale goes from 0 (black) to 100 (white), a* is the degree of red versus green, and b* the degree of yellow versus blue.
In industrial applications it is normally assumed that color differences of $\Delta E < 3$ correspond to small tolerances, from 3 to 6 are normal tolerances, and above 6 are large tolerances. However, the evaluation of quality and acceptability is highly subjective and depends on the application.
Secondly, the Goodness-of-fit Coefficient (GFC) [8], based on the inequality of Schwartz, was also used.

$$GFC = \frac{\sum_{\lambda} r(\lambda) r_{rec}(\lambda_j)}{\sqrt{\sum_{\lambda} \left[r(\lambda_j)\right]^2} \sqrt{\sum_{\lambda} \left[r_{rec}(\lambda_j)\right]^2}} \quad (7)$$

where $r(\lambda)$ are the spectral radiance (reflectance) components of the true curves, $r_{rec}(\lambda)$ are the estimated values and *n* is the number of wavelengths tested.
In fact, the GFC is the multiple correlation coefficient, the square root of $r_{rec}(\lambda)$'s spectral variance with respect to the original $r(\lambda)$. The GFC ranges from 0 to 1, with 1 corresponding to an exact duplicate of $r(\lambda)$. López-Álvarez et al. (8) suggested that colorimetrically accurate $r_{rec}(\lambda)$ require a GFC > 0.995; a ''good'' spectral fit requires a GFC > 0.999, and GFC > 0.9999 is necessary for an ''excellent'' fit.

Finally, the Root Mean Square Error (RMSE) was calculated, which is a very simple metric that has been used for spectral estimation evaluation in many studies [9]:

$$RMSE = \sqrt{\frac{1}{n}\sum_{\lambda}\left(r(\lambda) - r_{rec}(\lambda)\right)^2} \tag{8}$$

4. Results

Figure 12 shows the radiances and reflectances for some of the analysed samples computed by using the two former variants of the method. The true radiance/reflectance values measured with the spectroradiometer PR655 are also plotted. The curves obtained, both in terms of radiance and reflectance, were closer to the true values in the case of the variant I method whereas the variant II seemed to add a kind of offset to the measured values.

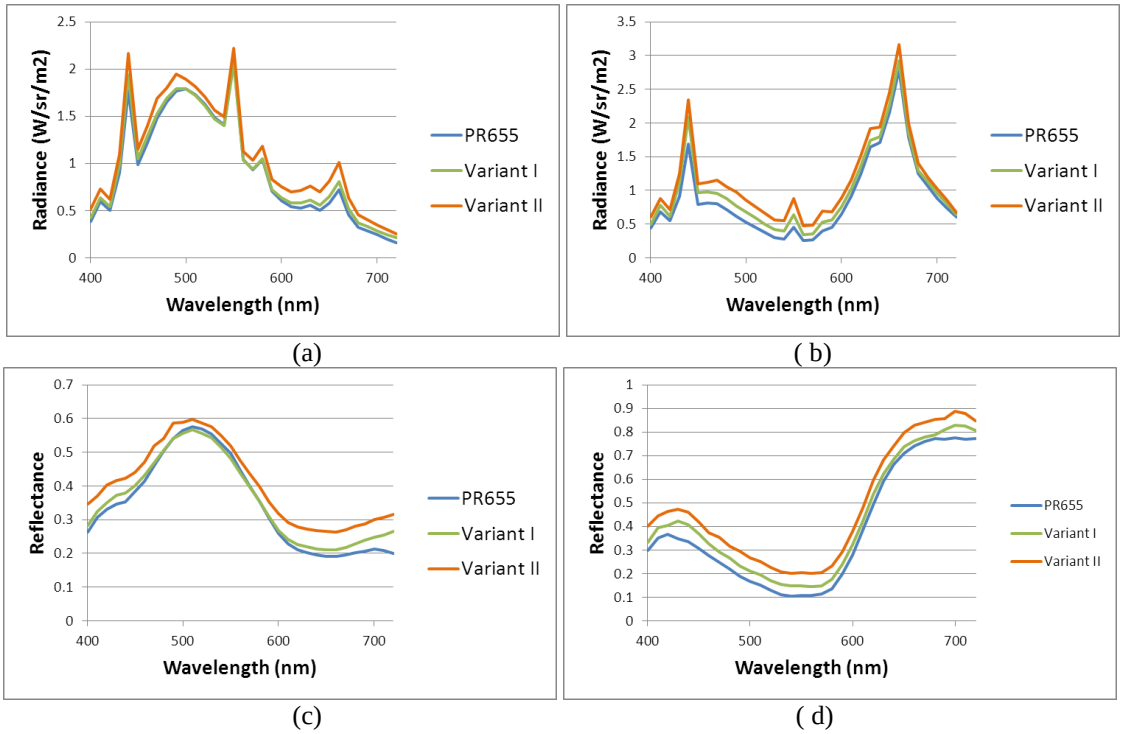

Figure 11. (a) Spectral radiance and (c) reflectance of Bluish green sample placed at the center of the scene. (b) Spectral radiance and (d) reflectance ofthe Magenta sample placed at the bottom-right corner of the scene.

In order to summarize the results obtained, Table 2 shows the statistics in terms of the colour difference (ΔE), Goodness-of-fit Coefficient (GFC), and Root-Mean-Square-Error (RMSE) between the true and estimated spectra for the two variants of the method applied and all samples analysed. As it can be seen again, better results were always obtained by means of the variant I. Variant I involves less calculations and processing of the acquired image and this could have an impact on the results. This could partially explain the better results obtained with this method. Furthermore, reflectances had better results than radiances whatever the method applied. The reason of that could be that radiance spectra had narrow peaks associated to the light source used in this study (fluorescent bulb with daylight emission) while reflectance spectra were linked to a more pronounced smoothness.

Focusing our attention on the best values obtained, that is, estimated reflectances by means of variant I, it can be seen that colour differences are larger than 6 units, i. e. far from the acceptable values. However, in terms of the GFC parameter, which accounts for the spectral fit along all the spectral range considered and not for perceived colour differences, the mean value obtained is of 0.995, which can be considered accurate enough.

Table 2. Statistics of the results in terms of radiance and reflectance. Values of color difference (ΔE), Goodness-of-fit Coefficient (GFC), and Root-Mean-Square-Error (RMSE) between the true and estimated spectra for the two variants (Variant I [VI] and II [VII]) of the method applied and all samples analysed are shown.

		ΔE		**GFC**		**RMSE**	
		VI	VII	VI	VII	VI	VII
Radiance ($W/m^2 \cdot sr$)	Orange	26.20	38.32	0.9907	0.9755	0.1324	0,2194
	Yellow green	18.60	30.68	0.9856	0.9768	0.1689	0.2623
	Bluish green	8.34	13.42	0.9872	0.9848	0.1844	0.2370
	Blue	15.34	35.13	0.9753	0.9464	0.1116	0.2299
	Magenta	8.86	19.18	0.9903	0.9855	0.1872	0.3152
	Mean	15,47	27,35	0,9858	0,9738	0,1569	0,2528
	Standard deviation	7,41	10,64	0,0063	0,0160	0,0334	0,0383
	Maximum	26,20	38,32	0,9907	0,9855	0,1872	0,3152
	Minimum	8,34	13,42	0,9753	0,9464	0,1116	0,2194
		ΔE		**GFC**		**RMSE**	
		VI	VII	VI	VII	VI	VII
Reflectance	Orange	17.79	26.35	0.9919	0.9791	0.0511	0.0786
	Yellow green	12.02	19.82	0.9957	0.9882	0.0401	0.0814
	Bluish green	4.35	7.71	0.9991	0.9963	0.0172	0.0583
	Blue	11.68	25.08	0.9905	0.9528	0.0271	0.0793
	Magenta	6.36	13.82	0.9980	0.9937	0.0427	0.0969
	Mean	10,44	18,56	0,9950	0,9820	0,0356	0,0789
	Standard deviation	5,29	7,83	0,0037	0,0176	0,0134	0,0137
	Maximum	17,79	26,35	0,9991	0,9963	0,0511	0,0969
	Minimum	4,35	7,71	0,9905	0,9528	0,0172	0,0583

5. Discussion

The multispectral system based on a LCTF provided useful spectral information of different samples both in terms of radiance and reflectance with high spatial resolution. The best results were achieved for reflectance, with a marked smoothness along the whole spectrum, and using the variant I method, which was simpler to implement. In this case the spectral fits could be considered acceptable. However, the system still presented some aspects that could be improved and that would help minimizing the colour difference values.

First of all it must be mentioned that the tunable filter suffered from a marked lack of uniformity in the transmittance profile, which did not depend on the incident angle of the incoming rays exclusively but also on the system itself, which showed a diagonal pattern (Figure 9). This was expected to be corrected during the processing step in which the flat field image was considered, however this was not enough. This lack of non-uniformity made impossible to use the whole dynamic range of the system as the results of Table I demonstrate, in which low mean DL were obtained if the condition of not saturating any pixel was considered.

Besides, the transmittance of the LTCF filter in the blue region (400-450 nm) was very low (less than a 5% against the 35% of the red channels). This was partially corrected by using larger exposure times in the blue channels; however this entailed more variation in the DL of the acquired images, providing a low signal-to-noise ratio which worsened the estimated spectral results. The signal-to-noise ratio could be improved by making use of an extra light source emitting more energy in the blue region.

Other factors to bear in mind are the appearance of second order peaks in the red region and in the near IR when the LCTF is working in the 400-450nm bands. The red peaks were assumed as an error and therefore this could directly affect the estimated spectral numbers. It should be also mentioned that some “ecos” in the images acquired between the 700-720nm channels were observed (Figure 12). This could be produced by these second order peaks described or also by misalignments between the IR cutoff filter and other parallel flat surfaces of the system such as those in the LTCF.

Regarding the optical design of the system a better integration between the lens, the LCTF and the camera should be done since some vigneting, although small, was still observed in the images. Moreover, there was a slight defocus between the different spectral channels of the

system. However, this is very difficult to solve due to the fact that if a different focus was used through each channel, other errors related with the repeatability in the position would arise. Besides, there would be an increment in the time needed for the scene capture.
Finally, it must be highlighted that all acquisitions were performed using indoor scenes with a high control of the illumination and the samples. The use of the system in outdoor scenes is still a goal which will be covered once resolved all the issued presented here.

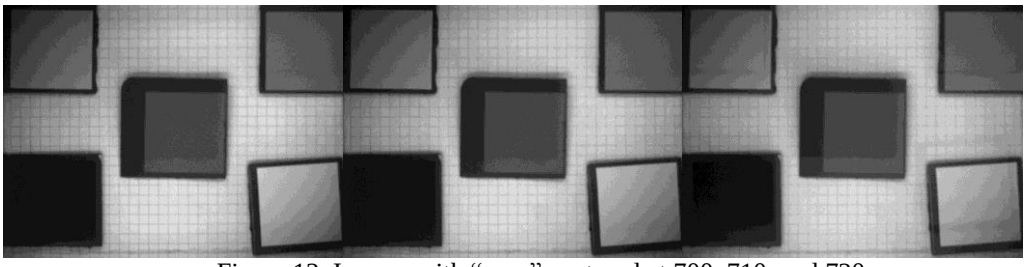

Figure 12. Images with "ecos" captured at 700, 710, and 720 nm

5. Conclusion

The multispectral system based on a LCTF developed in this study is a novel and compact portable system, which works readily and provides the spectral radiance and reflectance information of any pixel of the acquired scene. Beyond all possible improvements aforementioned, which will be carried out in future work, the use of the system brings great expectations in comparison with conventional spectrophotometric systems, which only provide spectral information integrated from a large area. Therefore, they are expected to be a valuable tool to be implemented in the industry, where many processes of production and control quality can benefit from their advantages.

Acknowledgments

This research was funded by the Spanish Ministry of Education and Science under grant DPI DPI2011-30090-C02-01, and by the European Union. I am indebted to my advisor, Prof. Meritxell Vilaseca for her help and encouragement throughout the course of this work, to Jaume Pujol for giving me the opportunity of doing this thesis, and to my lab partners, Xana and Jorge.

References

[1] Bowmaker R J, Dunn R J, Moynihan K B, Roper T J and Andrews M 2011 Construction of a practical hyperspectral image acquisition system. *Rev. Sci. Instrum.* 69, 1974-1977

[2] Bannon D 2009 Hyperspectral imaging: cubes and slices. *Nature Photonics* 3, 627 - 629

[3] Grahn HF & Geladi P 2007. Techniques and Applications of Hyperspectral Image Analysis. *John Wiley & Sons, England*

[4] Harold H S, Martin V, William JC 2000 Imaging spectroscopy using tunable filters: a review. *SPIE Proc*. 4056, 50-64

[5] Araújo Pinto PD 2007 Propriedades cromáticas em cenas naturais e a sua influência no olhar. PhD Thesis.

[6] Lasarte M 2007 Optimized algorithm for the spatial nonuniformity correction of an imaging system based on a CCD color camera. *Appl. Opt.* 46, 167–174

[7] Wyszecki G 1982 Color Science: concepts and methods, quantitative data and formula. *John Wiley & Sons, NY-USA*

[8] López-Álvarez M. A, Hernández-Andrés J, Romero J, Olmo F. J, Cazorla A, Alados-Arboledas L, 2008 Using a trichromatic CCD camera for spectral skylight estimation. *Appl. Opt*. 47, H31-38

[9] Imai F. H, Berns R. S 2000 Comparative analysis of spectral reflectance reconstruction in various spaces using a trichromatic camera system. *Jour. Imaging. Sci. and Technol*. 44, 280-377